Localization of scattering resonances in aperiodic Vogel spirals

F. Sgrignuoli,[1] R. Wang,[1] F. A. Pinheiro,[2] and L. Dal Negro[1,3,4,*]

[1]*Department of Electrical and Computer Engineering, Boston University, 8 Saint Mary's Street, Boston, Massachusetts 02215, USA*
[2]*Instituto de Fisica, Universidade Federal do Rio de Janeiro, Rio de Janeiro-RJ 21941-972, Brazil*
[3]*Division of Material Science and Engineering, Boston University, 15 Saint Mary's Street, Brookline, Massachusetts 02446, USA*
[4]*Department of Physics, Boston University, 590 Commonwealth Avenue, Boston, Massachusetts 02215, USA*

(Received 20 August 2018; revised manuscript received 17 January 2019; published 15 March 2019)

By using the dyadic Green's matrix spectral method, we demonstrate that aperiodic deterministic Vogel spirals made of electric dipoles support a light localization transition in three dimensions, an effect that does not occur in traditional uniform random media. We discover a light localization transition in Vogel spiral arrays embedded in three-dimensional space by evaluating the Thouless conductance, the level spacing statistics, and by performing a finite-size scaling. We probe light localization in the plane of the array by analyzing the behavior of the scattering resonances in three-dimensional space. This light localization transition is different from the Anderson transition because Vogel spirals are aperiodic deterministic structures characterized by nonuniform geometries. Moreover, this transition occurs when the vector character of light is fully taken into account, in contrast to what is expected for traditional uniform random media of pointlike scatterers. We show that light localization in Vogel arrays is a collective phenomenon that involves the contribution of multiple length scales. Vogel spirals are suitable photonic platforms to localize light thanks to their distinctive structural correlation properties that enable collective electromagnetic excitations with strong light-matter coupling. Our results unveil the importance of aperiodic correlations for the engineering of photonic media with strongly enhanced light-matter coupling compared to the traditional periodic and homogeneous random media.

DOI: 10.1103/PhysRevB.99.104202

I. INTRODUCTION

Understanding the localization of vector waves in dielectric systems provides exciting opportunities for the realization of more efficient sensors and active photonic platforms. Since the discovery by P. W. Anderson in 1958 that strong disorder can inhibit electronic transport [1], the quest for an optical counterpart of strong localization has motivated an intense research activity in photonic random media [2,3]. Random lasers [4,5], multiple scattering in random media [3,6–17], local density of states modification induced by multiple scattering [18,19], tuning and controlling of coupled-random modes [20–22], and speckle pattern information decoding [23–25] are some of the important results recently achieved in the field of disordered photonics. However, there is no unquestionable observation of a light localization transition in three-dimensional (3D) uniform random systems (i.e., in a full vectorial electromagnetic problem) so far [26–29]. The lack of materials with large enough refractive index values at optical frequencies and the presence of near-field coupling effects between scatterers in dense systems are often considered the main reasons preventing Anderson localization of light in homogeneous random media [27,30]. Moreover, due to the lack of simple design rules for efficient optimization, the applications of uniform random structures to optical engineering remain quite limited.

Aperiodic optical media, generated by simple deterministic mathematical rules, offer an alternative route to achieve light confinement with respect to uniform random systems. Aperiodic deterministic systems have recently attracted significant attention in the optics and electronics communities [31–34]. This is due, not only to their design advantages and compatibility with current nanofabrication technologies, but also to their distinctive optical behavior [34–39]. In particular, deterministic aperiodic structures display physical properties that cannot be found in either periodic or uniform random systems, such as anomalous transport [40–42] and fractal transmission spectra [43,44]. Moreover, the tunable structural complexity of aperiodic deterministic media leads to the formation of rich spectra of resonances, called critical modes [38,45,46], characterized by power-law envelope localization and multifractal field intensity oscillations [37–39,43]. Due to their unique functionalities, deterministic aperiodic designs have been successfully utilized in engineering applications for light emission and lasing [42], optical sensing [33,35], photodetection [36], nonlinear optical devices [47,48], as well as optical imaging [49].

In this paper we show that the large family of deterministic aperiodic Vogel arrays composed of electric dipoles can be conveniently designed to achieve a light localization transition in three dimensions. We prove that a transition from diffusive to localized regimes exists in planar Vogel spiral arrays embedded in 3D space by using the dyadic Green's matrix formalism [12–15]. The Green's matrix method has been applied to investigate Anderson localization of light in uniform disordered systems [6–17] and has allowed us to unveil the fundamental scattering and transport properties of aperiodic deterministic geometries [37–39].

*dalnegro@bu.edu

In this work we focus on open planar spiral structures as they are relevant architectures for experiments and applications where light can leak out through the array plane [34–36,50–52]. Therefore, the dimensionality of the electromagnetic problem is 3D but the geometrical support of the scattering arrays is two dimensional (2D). In such situations the electromagnetic field, which corresponds to a 3D scattering resonance, is not only spatially confined in the plane of the array, strongly depending on the geometry of its support, but it also leaks out from such a plane with a characteristic time proportional to the quality factor of the resonance. The discovered 3D light transition provides information on the localization of the waves in the plane of the support probed by the distinct behavior of 3D scattering resonances. As a result, this mechanism is different from a conventional 3D localization transition (e.g., Anderson localization transition) where waves are confined in all dimensions by the three-dimensional nature of the geometrical support.

We study light localization in Vogel spiral arrays with different geometrical parameters by evaluating the Thouless conductance, the level spacing distribution, and by performing a finite-size scaling. We show the existence of different classes of localized resonances that display spatial mode profiles recently discovered across the multifractal band edges of Vogel spirals performing 2D finite element method (FEM) simulations [53,54]. We explain the similarities between 3D and 2D scattering resonances in terms of light localization in Vogel spiral arrays that is generated by the nature of their geometrical supports. Moreover, we provide a comparison with respect to open uniform random planar arrays embedded in a 3D environment for both scalar as well as vector waves unveiling the full potential of aperiodic spatial correlations for the engineering of complex photonic media with more efficient light-matter interaction. Specifically, we demonstrate that light localization in Vogel spirals is driven by collective electromagnetic coupling effects that involve multiple length scales. For comparison, we show that vector wave localization is never achieved in planar homogeneous random systems, even when neglecting the near-field interaction term. This is shown by separately investigating the relative contributions of the different coupling terms that appear in the dyadic Green's propagator and by evaluating the Thouless conductance for sufficiently large scattering strengths. In summary, light localization transition in Vogel spirals occurs when the vector nature of light is taken into account, in contrast to the Anderson localization transition that it is limited to scalar waves [8,9]. Despite this important difference, the discovered light localization transition in Vogel spirals remarkably shares similar properties with the Anderson transition such as the crossover from level repulsion to the absence of level repulsion and the behavior of the Thouless conductance. Hence we conclude that structural correlations play a crucial role in light localization in Vogel spirals as compared to uniform random systems.

This paper is organized as follows. In Sec. II we describe the Green's matrix method and the Vogel spiral photonic array. In Sec. III we present and discuss our findings whereas Sec. IV is devoted to the conclusions.

II. METHODOLOGY: THE VOGEL SPIRAL PLATFORM AND THE GREEN'S MATRIX FORMALISM

Vogel spiral point patterns have been studied in physics, mathematics, botanics, and theoretical biology in relation to the fascinating geometrical problems offered by the field of phyllotaxis [37,54–57]. This class of deterministic aperiodic media is a powerful platform for nanophotonics and nanoplasmonic applications. Polarization-insensitive light diffraction [36], light-emission enhancement [50,51], enhanced second-harmonic generation [58], and omnidirectional photonic band gaps [59,60] are some of them. Vogel spiral geometries are characterized by diffuse scattering spectra like uniform random media but with circularly symmetric scattering rings that can be easily controlled by the spiral geometry [37,53,61]. By using simple generation rules, particle arrays with Vogel spiral geometry can be easily designed to produce a very rich structural complexity best described by multifractal geometry [53]. Moreover, Vogel spirals support distinctive scattering resonances that have been shown to encode well-defined numerical sequences in the orbital angular momentum of light, which have a great potential for device applications to singular optics and optical cryptography [62,63].

Vogel spiral arrays are defined in polar coordinates (r, θ) by the following parametric equations:

$$r_n = a_0\sqrt{n} \tag{1}$$

$$\theta_n = n\alpha, \tag{2}$$

where $n = 0, 1, 2, \ldots$ is an integer, a_0 is a positive constant called scaling factor, and α is an irrational number, known as the divergence angle [57]. This angle specifies the constant aperture between successive point particles in the array [55]. Since the divergence angle is an irrational number, Vogel spiral point patterns lack both translational and rotational symmetry. The divergence angle (α°, in degrees) can be specified by the choice of an irrational number ξ according to the relationship $\alpha^\circ = 360^\circ - frac(\xi) \times 360^\circ$ where $frac(\xi)$ denotes the fractional part of ξ. Vogel spirals with remarkably different structural properties can be obtained simply by selecting different values for the irrational number ξ. For instance, when ξ is equal to the golden mean $\xi = (1 + \sqrt{5})/2$ the corresponding divergence angle $\alpha \sim 137.508^\circ$ is called the "golden angle" while the resulting Vogel spiral structure is called the golden angle spiral, or GA spiral. This provides opportunities to tailor different degrees of aperiodic structural order in a very efficient way [37,61].

In this work, we primarily focus on four different types of Vogel spiral arrays introduced in Refs. [37,52,62], which are called GA spiral, τ spiral, π spiral, and μ spiral. They are generated according to Eq. (1) and Eq. (2) choosing the values $\xi = (1 + \sqrt{5})/2$, $\xi = (5 + \sqrt{29})/2$, $\xi = \pi$, and $\xi = (2 + \sqrt{8})/2$, respectively. The π spiral exhibits the lowest degree of structural order, followed by the μ spiral, the τ spiral, and the GA spiral [37,61]. This ordering reflects the smallest number of convergents (i.e., rational approximations) necessary to approximate the irrational number ξ in continued fractions at any level of accuracy [37,62].

We now investigate the spectral and wave localization properties of Vogel spirals using the Green's matrix method. This approach provides access to all the scattering resonances of a system composed of vector electric dipoles in vacuum and accounts for all the multiple scattering orders, so that multiple scattering process is treated exactly. In addition, this method allows for a full description of open 3D scattering resonances of large-scale structures at a relatively low computational cost if compared to traditional numerical methods such as finite difference time domain (FDTD) or FEM techniques. Each scatterer is characterized by a Breit-Wigner resonance at frequency ω_0 and width Γ_0 ($\Gamma_0 \ll \omega_0$). The quasimodes of this scattering system can be identified with the eigenvectors of the Green's matrix $\overleftrightarrow{G}$ which, for N vector dipoles, is a $3N \times 3N$ matrix with components [9]:

$$G_{ij} = i(\delta_{ij} + \tilde{G}_{ij}). \tag{3}$$

$\tilde{G}_{ij}$ has the form:

$$\tilde{G}_{ij} = \frac{3}{2}(1-\delta_{ij})\frac{e^{ik_0 r_{ij}}}{ik_0 r_{ij}}\left\{[\mathbf{U} - \hat{\mathbf{r}}_{\mathbf{ij}}\hat{\mathbf{r}}_{\mathbf{ij}}] - (\mathbf{U} - \mathbf{3}\hat{\mathbf{r}}_{\mathbf{ij}}\hat{\mathbf{r}}_{\mathbf{ij}}) \times \left[\frac{1}{(k_0 r_{ij})^2} + \frac{1}{ik_0 r_{ij}}\right]\right\} \tag{4}$$

when $i \neq j$ and 0 for $i = j$. k_0 is the wave vector of light, the integer indexes $i, j \in 1, \ldots, N$ refer to different particles, $\mathbf{U}$ is the 3×3 identity matrix, $\hat{\mathbf{r}}_{ij}$ is the unit vector position from the ith and jth scatter while r_{ij} identifies its magnitude. This method is suitable not only for the study of atomic clouds, as atoms are perfect dipoles, but also provides fundamental insights into the physics of periodic, aperiodic, and uniform random systems of small scattering particles [6–17,37–39]. The Green's matrix (3) is a non-Hermitian matrix. As a consequence, it has complex eigenvalues Λ_n ($n \in 1, 2, \ldots, 3N$) [12,13]. The real and the imaginary part of Λ_n are related to the detuned scattering frequency $(\omega_0 - \omega_n)$ and to the scattering resonance decay Γ_n both normalized with respect to the resonant width Γ_0 of an isolated dipole [9–11]. In the following, we define $\hat{\omega}_n = (\omega_0 - \omega_n)/\Gamma_0$.

In order to establish light localization, we have analyzed two parameters. The first parameter characterizes the degree of spectral overlap between different optical resonances and it is called Thouless conductance g [64,65]. The second parameter quantifies the sensitivity/insensitivity of scattering resonances with respect to a perturbation of the system boundary conditions and it is known as the β parameter. In order to prove a light localization transition we have applied two criteria. First, the g conductance, which is proportional to the scattering mean free path of the system, must decrease when increasing the scattering strength, i.e., increasing the optical density $\rho\lambda^2$. Here ρ is the number of particles per unit area while λ is the optical wavelength. Second, the scaling of the β parameter with respect to the logarithmic conductance ($\beta = \beta[\ln(g)]$) must show a critical point $q_c = \ln(g_c)$ at which β vanishes, i.e., the Thouless conductance does not depend on the system size L [66,67]. Moreover, we have corroborated our analysis by showing a crossover from level repulsion to the absence of level repulsion of the level spacing statistics (see Appendices E for details).

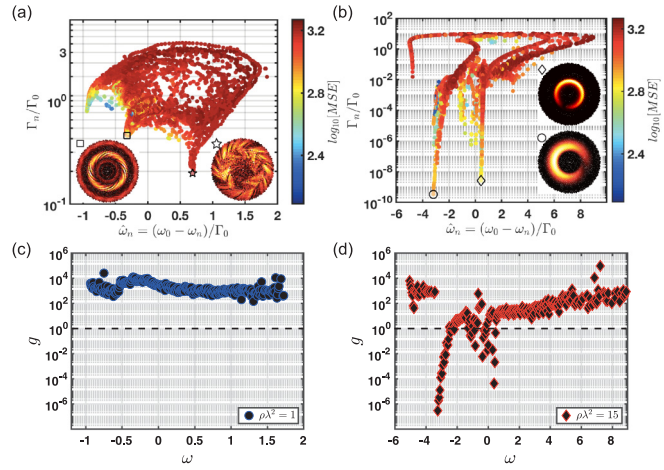

FIG. 1. Eigenvalues of the Green's matrix (3) are shown by points on the complex plane for 2000 electric point dipoles arranged in a GA Vogel spiral geometry. Panels (a) and (b) refer to an optical density of 1 and 15, respectively. Scattering resonances with very small decay rates ($\Im[\Lambda_n] = \Gamma_n/\Gamma_0 \ll 1$) appear only when $\rho\lambda^2 = 15$. The data are color coded according to the $\log_{10}$ values of the MSE. Insets: spatial profiles of representative quasimodes. Panels (c) and (d) show the frequency dependence of the Thouless conductance g when $\rho\lambda^2$ is equal to 1 and 15, respectively. The dashed-black lines identify the threshold of the diffusion-localization transition.

Within the Green's matrix formalism, the Thouless conductance is defined as the ratio of the dimensionless lifetime $(\delta\omega)^{-1} = 1/\Im[\Lambda_n]$ to the spacing of nearest dimensionless resonant frequencies $\Delta\omega = \Re[\Lambda_n] - \Re[\Lambda_{n-1}]$ [9]. In order to study the behavior of g as a function of the resonance frequencies, we have subdivided, for each value of the scattering strength $\rho\lambda^2$, the range of resonance frequencies in 300 equispaced intervals. This allows us to consider the average value of g within each subinterval and to obtain its frequency dependence by plotting the average values associated to each subinterval. The Thouless conductance g can be written in terms of the eigenvalues of the Green's matrix as

$$g = g(\omega) = \frac{\overline{\delta\omega}}{\Delta\omega} = \frac{(\overline{1/\Im[\Lambda_n]})^{-1}}{\Re[\Lambda_n] - \Re[\Lambda_{n-1}]}, \tag{5}$$

where $\overline{\{\cdots\}}$ indicates the average of g over each frequency subinterval. The frequency ω is the central frequency of each subinterval used to sample the $\Re[\Lambda_n]$ axes. Differently from the uniform random scenario [6–17,68], we do not perform any average with respect to different geometry configurations because Vogel spirals are deterministic structures.

III. RESULTS AND DISCUSSIONS

We will first consider the case of $N = 2000$ electric vector dipoles arranged in a GA Vogel spiral configuration. The 3N × 3N Green's matrix (3) is diagonalized numerically and the Thouless conductance g, defined by Eq. (5), is calculated as a function of the frequency ω for different values of $\rho\lambda^2$. Figures 1(a) and 1(b) show the distribution of the resonant complex poles Λ_n, color coded according to the $\log_{10}$ values

of the mode spatial extent (MSE), when the optical density is set equal to 1 and to 15, respectively. The MSE parameter characterizes the spatial extent of a photonic mode [20].

At low optical density ($\rho\lambda^2 = 1$), the system is in the delocalized regime. The complex eigenvalue distribution does not show the formation of any long-lived resonances with $\Gamma_n/\Gamma_0 \ll 1$. Consistently, the spatial profiles of the modes in this regime are delocalized across the array. For example, two representative eigenvectors that correspond to the smallest decay rates around $\hat{\omega}_n \sim -0.3$ (white-square marker) and $\hat{\omega}_n \sim 0.8$ (white-pentagram marker), are shown in the inset of Fig. 1(a). Expectedly, we found that the Thouless conductance is always larger than one in this case, as shown in Fig. 1(c).

However, at large optical density ($\rho\lambda^2 = 15$), the situation is completely different. Long-lived resonances appear and a significant fraction of the complex eigenvalues of the Green's matrix have a very small decay rate ($\Gamma_n/\Gamma_0 \ll 1$). For comparison, no such long-lived resonances appear in uniform random media when the vector nature of light is taken into account (see Appendix A and Refs. [8,9,16] for more details). We show the spatial profiles of two representative eigenvectors in the inset of Fig. 1(b) and we report in Fig. 1(d) the Thouless conductance as a function of frequency. These findings clearly demonstrate that the system reached the localization regime at large optical density, namely the eigenvectors are radially confined and $g(\omega) < 1$. We notice that the long-lived resonances shown in Fig. 1(b) are clustered around two "tail regions" that appear at the frequency positions where g becomes lower than one [see Fig. 1(d)].

Two other important features arise at sufficiently large optical density: the existence of a spectral gap region and the absence of subradiant "dark" states, also called proximity resonances, in the complex distribution of the eigenvalues [12,37,69]. Proximity resonances are subradiant states localized around pairs of scatterers and can be identified in random systems by their typical spiral distributions in the complex eigenvalue plane and are characterized by MSE=2 [8,12,68]. The absence of proximity resonances in Vogel spiral systems was originally reported in Ref. [37] and attributed to the more regular structure of Vogel spirals compared to random media. This can be understood based on the fact that, for a given optical density, the first-neighbor distance of the particles is, on average, larger in the case of Vogel spirals. Indeed, we have previously shown that the probability distribution of first-neighbor distances is non-Gaussian for Vogel spirals and characterized by long tails [34,37,53,70]. More specifically, the mean value of the first-neighbor distances of the GA spiral is $\bar{\delta}^{1st} = 1.70 \pm 0.02$ (in units of the scaling factor a_0). In contrast, uniform random point patterns, with the same density, are characterized by a Poissonian first-neighbor distribution [71] with larger fluctuations: $\langle \bar{\delta}^{1st} \rangle_e = 0.89 \pm 0.47$. Here $\langle \cdots \rangle_e$ indicates the average over two hundreds different point pattern realizations. Therefore, for a given optical density the probability of observing two very close particles is much larger for the uniform random patterns (see Appendix B for more details). Interestingly, these fluctuations increase up almost 20% in the π spiral configuration, which in fact is the spiral with the lowest degree of structural order among the ones considered in this work. The lack of significant

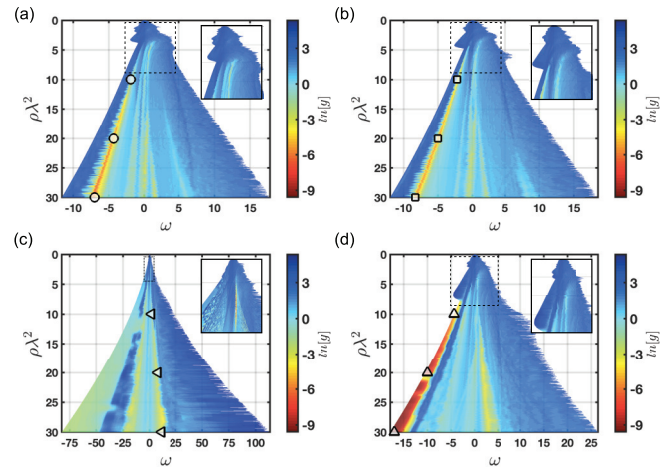

FIG. 2. Highly resolved maps of the logarithmic values of the averaged Thouless conductance are evaluated for different values of the optical density $\rho\lambda^2$ as a function of ω. The data of panels (a)–(d) are color coded according to ln[g] and refer to the GA spiral, τ spiral, π spiral, and μ spiral, respectively. Each Thouless conductance $g(\omega)$ is characterized by 300 points. These maps are calculated in the range $\rho\lambda^2 = [0.1, 30]$ with a resolution of 0.1. Insets: enlarged view of the threshold region for the diffusion-localization transition. Green-red-yellow features identify the appearance of localized resonances that follow clear dispersion branches with respect to ω. Different markers identify the classes of localized resonances that produce the stronger localization feature in the considered Vogel spirals.

contributions from the subradiant resonances in Vogel spiral has profound consequences for light localization and simplify considerably the analysis of g and the β scaling compared to uniform random systems where the proximity resonances need to be carefully removed [8–10].

In order to gain more insights on the localization transition we study the logarithm of the averaged Thouless conductance for different values of the optical density (starting from 0.1 up to 30 with a resolution of $\rho\lambda^2 = 0.1$) as a function of ω. In this way, highly resolved maps of the quantity $\ln[g] = \ln[g(\omega, \rho\lambda^2)]$ can be obtained. The results of this analysis are summarized in Figs. 2(a)–2(d) for the GA, τ, π, and μ spirals, respectively. The data are color coded according to the logarithmic values of the Thouless conductance. The diffusion-localization threshold is defined according to $\ln[g(\omega, \rho\lambda^2] = 0$ and it is identified by the cyan color. Insets display enlarged views of the threshold region for the diffusion-localization transition. Localization begins to take place at $\rho\lambda^2 \sim 3.5$ for all the geometries except for the less correlated π spiral configuration, whose threshold occurs at $\rho\lambda^2 \sim 2$. While this analysis focused on spirals with $N = 2000$, we have numerically verified that the results are robust with respect to system size ($N = 500$–4000) and the frequency resolution used in the computation of the Thouless conductance g.

The appearance of localized resonances, identified by the green-red-yellow features in Fig. 2, shows a clear dispersion branch with respect to the frequency ω in all the investigated geometries. These features cannot be obtained in a uniform random medium where the attainable value of the Thouless conductance are always larger than one [8,9]. (See also

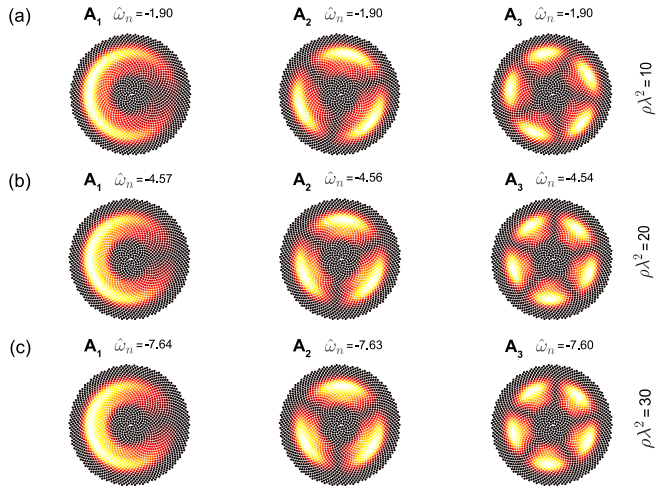

FIG. 3. Representative spatial distributions of the Green's matrix eigenvectors that belong to the class of scattering resonances that produce the stronger localization feature in the GA spiral. A_1, A_2, and A_3 identify the first three resonances with the lower decay rates ($\Gamma_n/\Gamma_0 \ll 1$). Panels (a)–(c) show these quasimodes when the optical density $\rho\lambda^2$ is fixed to 10, 20, 30, respectively. The spectral positions of these quasimodes are identified by the white-circle markers in Fig. 2(a).

Appendix A for a detailed comparison with respect to the vector and the scalar model of uniform random planar arrays embedded in a 3D space with the same optical density of Vogel spirals). In Vogel spirals different classes of localized resonances are clearly visible in Fig. 2.

To achieve a deeper understanding on the nature of these localized scattering resonances that belong to different dispersion branches, we have systematically analyzed the spatial distributions of a few representative examples identified by the markers shown in Fig. 2. These markers identify the behavior of the class of scattering resonances that produce the stronger localization feature in the considered Vogel spirals. We first focus on the type of resonances highlighted with the white-circle markers in Fig. 2(a). The spatial distributions of eigenvectors of the Green's matrix corresponding to the three resonances with the lower decay rates are labeled in Fig. 3 as A_1, A_2, and A_3, respectively. In Figs. 3(a)–3(c) the optical density $\rho\lambda^2$ is fixed to 10, 20, and 30, respectively. For each one of them, the frequency of the scattering resonance $\hat{\omega}_n$ is also indicated. It is clearly shown that exactly the same spatial profile is retrieved when scanning along the dispersion branches for all the three resonances A_1, A_2, and A_3. The effect of increasing the optical density $\rho\lambda^2$ is simply to produce a frequency shift in the complex scattering plane. Interestingly, we notice that the spatial profiles of the scattering resonances shown in Fig. 3 agree very well with what has been previously reported based on the 2D FEM method [53,54,70], demonstrating the power of the more efficient Green's matrix approach. Specifically, in our previous 2D numerical studies we discovered that the localized modes of Vogel spirals have a quality factor that scales linearly with the frequency, which allowed us to classify them into different classes [53,54,70]. The modes belonging to the same class have similar spatial patterns and each one of them has a degenerate counterpart characterized by a complementary spatial profile. We now report a complete classification of the Vogel spiral modes based on the more systematic and general dyadic Green's matrix analysis that provides access to all the scattering resonances that exist, for a given optical density, in an open 3D electromagnetic system. As an example, the three types of resonances shown in Fig. 3 have exactly the same spatial profiles that correspond to band edge modes of class A, as defined in Refs. [53,54,70]. Moreover, also the degenerate modes of A_1, A_2, and A_3 can be identified by using the dyadic Green's matrix formalism. They occur exactly at the same $\hat{\omega}_n$ and they are characterized by a complementary spatial profile. This comparison demonstrates also that light localization in Vogel spirals is produced at the band edge due to the strongly-fluctuating (multifractal) dispersion in the density of states [53]. Exactly the same conclusions are obtained for the τ spiral, π spiral, and μ spiral (see Appendix C for more details).

In order to understand the similarities between the spatial distribution of the localized scattering resonances of Vogel spirals in 2D and 3D environments, we have calculated their spatial distributions and average modal lifetimes using the cylindrical Hankel functions, which describes a 2D electromagnetic problem, as well as a dyadic Green's matrix method, which describes 3D electromagnetic systems. We find that localized eigenmodes supported by open Vogel spiral arrays embedded in a 3D environment correspond very well to the ones obtained for a 2D electromagnetic problem at large optical densities. This is due to the fact that the geometrical support is the same and that light localizes in the plane of the spirals. Indeed, the 2D modes survive in a totally open 3D environment if the optical density is large enough to induce light localization in the plane of the support. On the other hand, Fig. 1(a) demonstrates that 2D modes do not correspond to the scattering resonances supported by open Vogel spiral arrays embedded in 3D space in the diffusive regime. In this case the scattering resonances are short lived and hence very different from the 2D ones [see inset of panel (a) of Fig. 1]. However, 3D scattering resonances have much smaller average modal lifetimes due to the open nature of the 3D space with respect to their 2D counterparts (see Appendix F for details).

Motivated by the similarities between the light localization transition in Vogel spirals and the Anderson light localization transition in random media characterized by a Gaussian (uniform and isotropic) disorder model, we perform the scaling analysis of localization [9] for Vogel spirals. For the Anderson localization in random media, this analysis predicts that a phase transition between localization and diffusion exists only in 3D, whereas the system is expected to be in the localized regime in lower dimensions for sufficiently large systems [66]. Therefore, the diffusive and localized regimes are separated by a critical point, called the "mobility edge." The scaling analysis is characterized by only one parameter, the Thouless conductance g. According to the scaling theory of Anderson localization, the dependence of the conductance on the system size can be described by the β function [66]:

$$\beta(\ln[g]) = \frac{d\ln[g]}{d\ln[L]}, \tag{6}$$

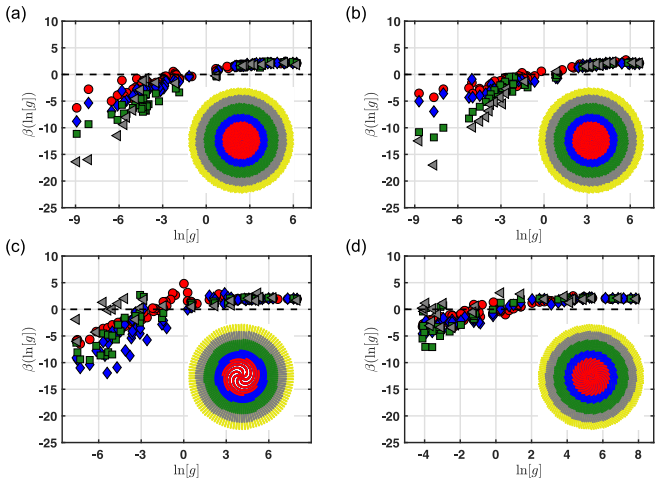

FIG. 4. The β scaling analysis is performed by increasing the number of scatters from $N = 500$ up to $N = 4000$. Panels (a)–(d) display the results of this scaling for the GA spiral, τ spiral, π spiral, and μ spiral, respectively. Different markers correspond to calculations of the β function for all the possible combinations of N. Red circles, blue diamonds, olive squares, and gray triangles determine the combination of $N = 500$ versus $N = 1; 2; 3; 4 \times 10^3$, $N = 1000$ versus $N = 2; 3; 4 \times 10^3$, $N = 2000$ versus $N = 3; 4 \times 10^3$, and $N = 3000$ with respect to $N = 4 \times 10^3$, respectively. The dashed-black lines identify the β parameter transition threshold. Insets: set of different Vogel spirals generated by increasing the number of scatters: $N = 4000$ (yellow), $N = 3000$ (gray), $N = 2000$ (olive), $N = 1000$ (blue), and $N = 500$ (red).

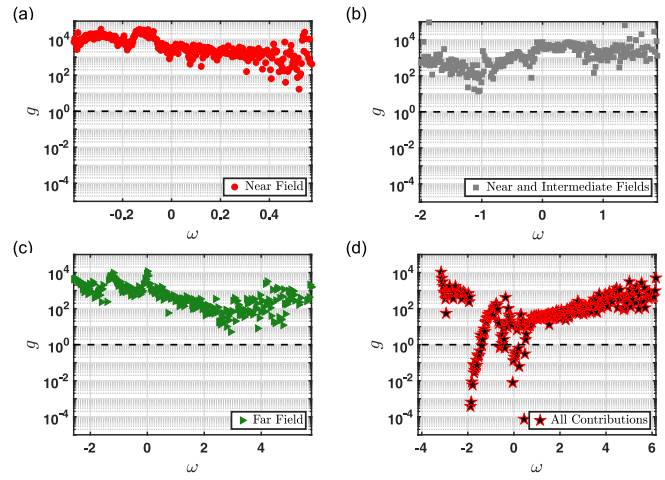

FIG. 5. Panels (a)–(d) display, in a semilog-y scale, the frequency dependence of g after diagonalizing the $3N \times 3N$ Green's matrix associated to only the near-field term, the near-field term plus the intermediate-field contribution, the far-field term only, and all the coupling contributions, respectively. These data refer to the GA spiral when the optical density $\rho\lambda^2 = 10$. The dashed-black lines identify the threshold of the diffusion-localization transition $g = 1$. Similar results are obtained for all the other investigate Vogel spirals and compared with uniform random media in Appendix D.

where L is the product of the wave vector k_0 and the system size R, which is the maximum radial coordinate of the spiral (see insets of Fig. 4). Equation (6) assumes that Thouless conductance g is a continuous and monotonic function of L. Figures 4(a)–4(d) display the results of the scaling analysis applied to GA spiral, τ spiral, π spiral, and μ spiral, respectively, by increasing the number of scatters from $N = 500$ up to $N = 4000$. Even though a scaling theory of localization for nonuniform systems is currently missing, the analysis reported in Fig. 4 suggests the existence of a localization transition in Vogel structures because the sign of β changes from negative to positive, consistently with the one-parameter scaling theory. However, deeper theoretical investigations, beyond the scope of the present work, are necessary to fully understand the nature of the discovered light transition probed by the 3D scattering resonances of Vogel spirals.

Our results demonstrate a light localization transition supported by open Vogel spirals planar arrays embedded in three dimensions. This phenomenon cannot occur in traditional uniform random media when the vector nature of light is taken into account within the Green's matrix formalism (see Refs. [8,9] and Appendices A and D for more details). These results put into evidence the main difference between the light localization transition in Vogel spirals and the Anderson localization transition, which occurs only in the scalar approximation for pointlike electric dipoles [8,9]. However, the light localization transition in Vogel spirals remarkably shares similar properties with the Anderson transition such as the crossover from level repulsion to the absence of level repulsion (as demonstrated in Appendix E) and the behavior of the Thouless conductance. It is important to note that in our study, although the dipoles are arranged in planar Vogel spiral arrays, the electromagnetic field is not only confined in the plane but it also leaks out to free space according to the quality factors of the scattering resonances (see Appendix F for more details). Therefore such systems are truly open scattering 3D systems. In contrast, in a two-dimensional problem the electromagnetic field is uniform along the z axis and its propagator is the 2D Green's function [15–18].

In order to investigate the role of cooperative effects in the light localization of Vogel spirals we have decomposed the Green's matrix of Eq. (4) into the sum of three coupling terms. Each term describes different electromagnetic coupling regimes proportional to $1/r_{ij}$, $1/r_{ij}^2$, and $1/r_{ij}^3$, corresponding to long-range, intermediate-range, and short-range electromagnetic interactions, respectively. We separately investigated these different contributions of the dyadic Green's propagator and, for each one of them and for their different combinations, we evaluated the Thouless conductance for an optical density $\rho\lambda^2 = 10$. Figure 5 summarizes our results for the case of a GA spiral (similar results are obtained for all the other investigated Vogel spirals and compared with uniform random media in Appendix D). Panels (a)–(d) show the frequency dependence of the Thouless conductance g obtained by using Eq. (5) after diagonalizing the 3N × 3N Green's matrix associated to only the near-field term, the near-field term plus the intermediate-field contribution, the far-field term only, and all the coupling contributions, respectively. Light localization, characterized by $g < 1$, occurs only when all the coupling terms, including the near-field regime, are simultaneously taken into account. Therefore, our results demonstrate that light localization in Vogel spirals results

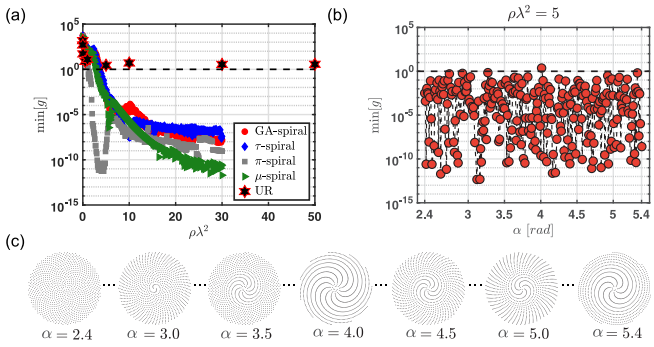

FIG. 6. (a) The minimum value of the Thouless conductance as a function of $\rho\lambda^2$ is reported in a semilog-y scale. Different markers identify the different analyzed structures. Red-circle markers, blue-diamond markers, gray-square markers, olive-triangle markers, and red/black-hexagram markers refer to the GA spiral, τ spiral, π spiral, μ spiral, and to the uniform random configuration (i.e., UR), respectively. 10 different disorder realizations are considered for the UR analysis. (b) min[g] behavior as a function of the divergence angle α (expressed in radiant) when $\rho\lambda^2 = 5$. 300 Vogel spirals, with remarkably different structural correlations, are generated between $\alpha = 2.4$ rad and $\alpha \sim 5.4$ rad. Some representative Vogel spiral geometries are shown in panel (c). The dashed-black lines identify the threshold of the diffusion-localization transition $g = 1$.

from a collective coupling effect that involves multiple length scales. Remarkably, we also demonstrate that vector wave localization is never achieved in uniform random systems with a planar support, even neglecting the near-field interaction term (see Appendices A and D for more details).

The effect of the optical density on the minimum value of the Thouless conductance g is illustrated in Fig. 6(a) where we also compare with the case of planar uniform random media, referred to as UR in the legend. All the structures have $N = 2000$ interacting particles and the random system's results are averaged over 10 different realizations. Moreover, in order to eliminate the contribution of proximity resonances from the analysis of the random configuration, we have carefully neglected the resonances with $MSE = 2$ [8,12,68]. Figure 6(a) shows that light localization never appears in uniform random arrays. This analysis is performed for different values of $\rho\lambda^2$ up to 50. In contrast, all the Vogel spirals exhibit light localization starting from a threshold value of $\rho\lambda^2 \geqslant 2$, as previously discussed. The π spiral configuration, whose geometry is the least correlated, displays the lowest localization threshold as well as the minimum g value. In order to generalize our findings to a much larger set of Vogel spirals, we compute in Fig. 6(b) the minimum value of g at optical density $\rho\lambda^2 = 5$ for 300 different Vogel spirals obtained by continuously varying the polar divergence angle α defined in Eq. (2). All these structures are generated with a divergence angle that linearly interpolates between the GA spiral and the π spiral. Some representative geometries are shown in Fig. 6(c). These data demonstrate that vector wave localization is a very robust feature of Vogel spiral arrays that can be achieved for many different choices of the divergence angle α. The results of our paper clearly establish the relevance of controllable aperiodic correlations for the engineering of photonic scattering platforms with strong light-matter interaction.

IV. CONCLUSIONS

In summary, we have demonstrated a light localization transition supported by Vogel spiral planar arrays embedded in three dimensions by means of the dyadic Green's matrix method. Specifically, a clear transition from the diffusive to the localized regime, different from the Anderson localization transition in three dimensions, is discovered by evaluating the Thouless conductance, the level spacing statistics, and by performing a finite-size scaling analysis of the scattering resonances. This transition is a result of the complex interplay between the nature of the 2D geometrical support and wave propagation in three dimensions. Different classes of localized scattering resonances in Vogel spirals with distinctive spatial distributions have been identified and analyzed. By decomposing the dyadic field propagator in its different components we show that light localization in Vogel arrays originates from collective electromagnetic coupling involving the contributions of multiple length scales. All these effects do not occur in traditional uniform random media. Our results unveil the importance of structural correlations in deterministic aperiodic photonic media for the design of localized states with strongly enhanced light-matter interactions. In addition, our findings may open vistas for the engineering of mesoscopic transport and localization phenomena and should encourage deeper investigations of photonic devices based on deterministic aperiodic architectures.

ACKNOWLEDGMENTS

This research was sponsored by the Army Research Laboratory and was accomplished under Cooperative Agreement No. W911NF-12-2-0023. The views and conclusions contained in this document are those of the authors and should not be interpreted as representing the official policies, either expressed or implied, of the Army Research Laboratory or the U.S. Government. The U.S. Government is authorized to reproduce and distribute reprints for Government purposes notwithstanding any copyright notation herein. F.A.P. thanks the Brazilian agencies CNPq, CAPES, and FAPERJ as well as The Royal Society-Newton Advanced Fellowship (Grant No. NA150208) for financial support.

APPENDIX A: PLANAR UNIFORM RANDOM CONFIGURATION

The relevant features of light localization properties of uniform random arrays are presented in this Appendix. By following the procedure presented in Sec. II, we have evaluated the complex eigenvalues distributions of 10 different realizations of 2000 uniformly random distributed scatterers on a plane. Moreover, the spectral and optical properties of matrix (3), which takes into account the vector nature of light, were compared with those of its scalar approximation [9]

$$G_{ij} = i\delta_{ij} + (1 - \delta_{ij})\frac{e^{ik_0 r_{ij}}}{k_0 r_{ij}}. \tag{A1}$$

Figures 7(a) and 7(b) display the complex eigenvalues distributions obtained after diagonalizing the matrix (3) and its scalar approximation (A1) for $\rho\lambda^2 = 30$, respectively. In

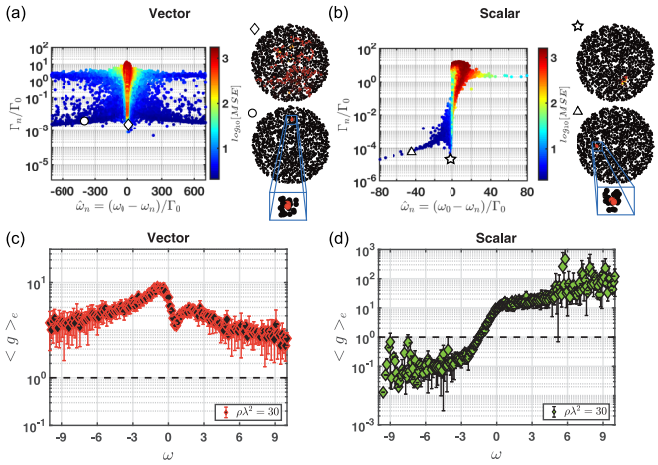

FIG. 7. Panels (a) and (b) display the complex eigenvalues distributions of 10 different random realizations of the Green's matrix defined by matrix (3) and matrix (A1), respectively. The data are color coded according to the $\log_{10}$ values of the MSE. Insets: spatial profiles of representative quasimodes. Panels (c) and (d) show the frequency dependence of the Thouless conductance g for the vector and scalar model, respectively. These data are produced by fixing $\rho\lambda^2 = 30$. The dashed-black line identifies the threshold of the diffusion-localization transition $g = 1$. The error bars are calculated as the standard deviation of the Thouless conductance g evaluated for the different disorder realizations.

random media, long-lived resonances do not appear when the vector nature of light is taken into account. Consistently, the spatial profiles of the Green's matrix eigenvectors corresponding to the resonances with the lower decay rates are delocalized across all the structure (see the representative quasimode shown in the inset of Fig. 7(a)). On the other hand, the situation is completely different in the scalar configuration. Long-lived resonances are clustered around one band of localized quasimodes near $\hat{\omega}_n \sim -2.5$. The spatial distributions of quasimodes of the Green's matrix corresponding to this "tail region" are localized between several particles, as shown in the inset of Fig. 7(b) for a representative scattering resonance (star marker).

This analysis, inspired by Ref. [9], is confirmed by the frequency dependence of the Thouless conductance g. The conductance is evaluated by using Eq. (5), which has been modified to take into account the effect of the different disorder realizations [9,10]. Moreover, the contribution of subradiant resonances (for which $MSE = 2$) is omitted from this analysis [8–10]. As expected, Fig. 7(c) shows that the Thouless conductance g is always larger than one when the vector nature of light is taken into account. On the contrary, the frequency dependence of g shows a transition from $g < 1$ to $g > 1$ in the scalar case [see (Fig. 7(d)]. These data are obtained by fixing $\rho\lambda^2 = 30$. This analysis confirms the results of Refs. [8,9] obtained for a 3D random distribution of electric dipoles. However, in our case localization is less pronounced if compared to the case treated in Refs. [8,9] for the scalar model. This is due to the fact that in open random arrays leakage through the system plane results in more lossy channels if compared with the corresponding 3D case.

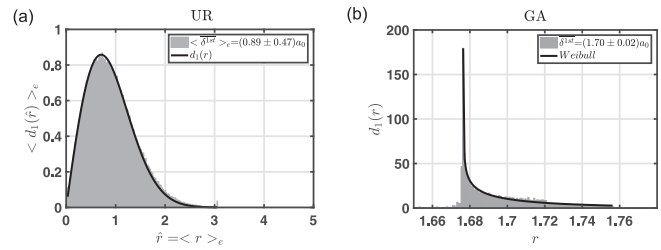

FIG. 8. Panel (a) and (b) displays the first-neighbor probability density function an homogeneous Poisson process and a GA spiral, respectively. The black lines are the corresponding analytical density functions obtained by using Eq. (B1) and the Weibull distribution, respectively. In the homogeneous Poisson process two hundred different realizations, with the same density of the GA spiral, are considered. All these data are in units of the scaling factor a_0 (see Eq. 1).

APPENDIX B: FIRST-NEIGHBOR PROBABILITY DENSITY FUNCTION ANALYSIS

In order to gain more insights on why proximity resonances are absent in Vogel spiral point patterns we study the properties of the first-neighbor probability density function of a GA spiral as compared to homogeneous Poisson point pattern. It is important to remember that the first-neighbor probability density function is a measure of the spatial uniformity of a given point pattern [37,71]. Figures 8(a) and 8(b) show the results of this analysis as a function of the spacing parameter r. Figure 8(a) is the result of an average over 200 different homogeneous Poisson patterns with exactly the same density of the GA spiral. The results of Fig. 8 clearly demonstrate that the GA spiral is characterized by a more regular structure as compared to random media. Indeed, the probability density function of a GA spiral is extremely peaked around the mean

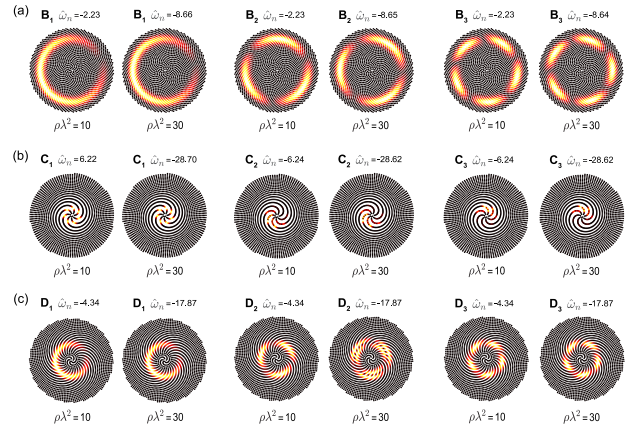

FIG. 9. Representative spatial distributions of the Green's matrix eigenvectors that belong to the class of scattering resonances that produce the stronger localization feature in the τ spiral (panel (a)), π spiral (panel (b)), and μ spiral (panel (c)), respectively. B_j, C_j, and D_j (with $j = 1, 2, 3$) identify the first three resonances with the lower decay rates ($\Gamma_n/\Gamma_0 \ll 1$). Moreover, panels (a)–(c) report these quasimodes when the optical density $\rho\lambda^2$ is fixed to 10 and 30. The spectral positions of these scattering resonances are identified by the different markers of Figs. 2(b) and 2(d).

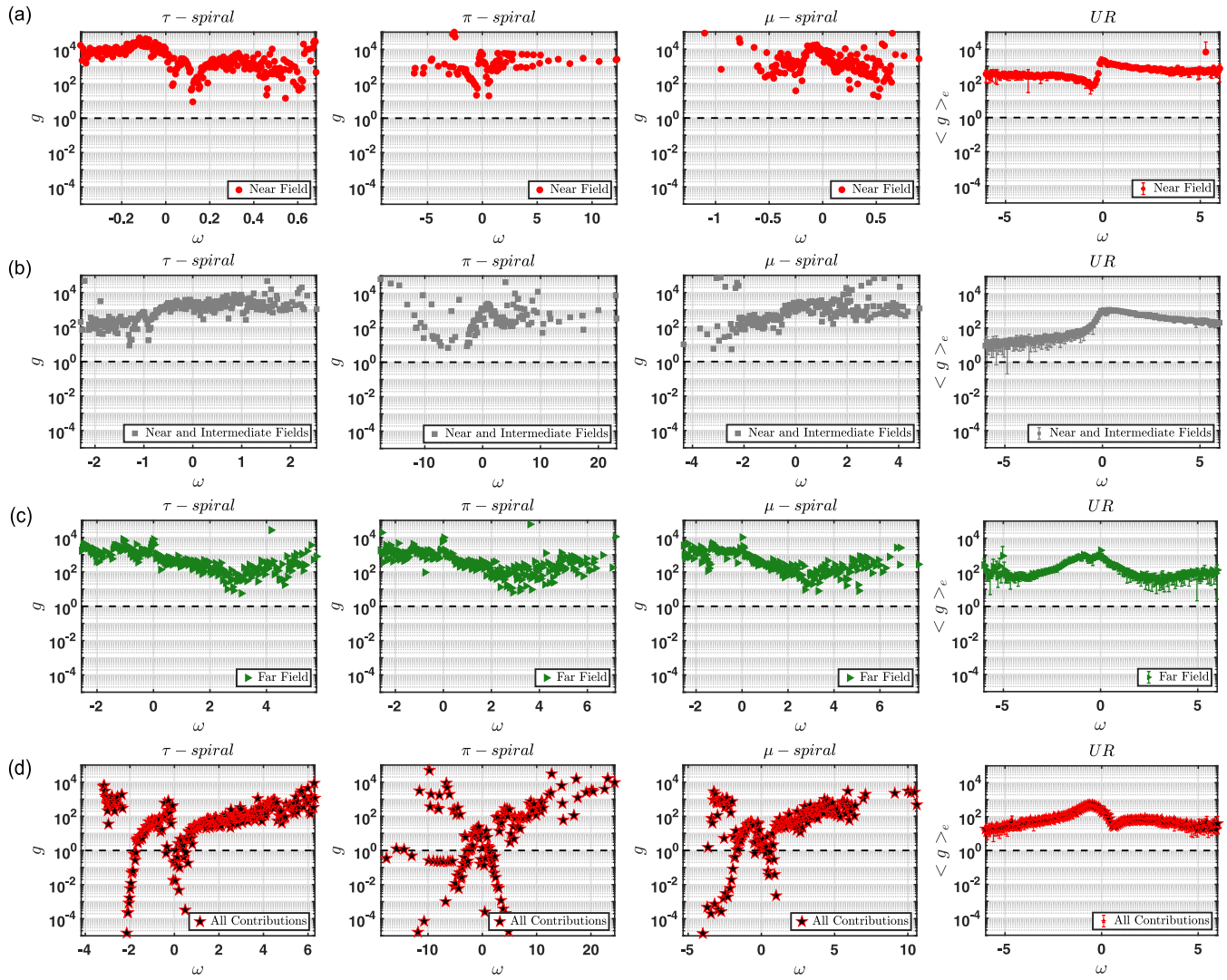

FIG. 10. Semilog plots of the Thouless conductance, as a function of ω, obtained by using Eq. (5) after diagonalizing the $3N \times 3N$ Green's matrix associated to only the near-field term (panel (a)), the near-field term plus the intermediate-field regime (panel (b)), the far-field term only (panel (c)), and all the coupling contributions (panel (d)) for the τ, π, μ spirals as compared to the UR configuration. This analysis is performed by fixing $\rho\lambda^2$ equal to 10. The error bars are evaluated as the standard deviations of the Thouless conductances calculated for 10 different disorder realizations. The dashed-black lines identify the threshold of the diffusion-localization transition $g = 1$.

value of the first-neighbor distances and it is very well reproduced by considering a Weibull distribution fitting function, as highlighted by the black line of Fig. 8(b). On the contrary, the UR configuration is characterized by a Poissonian first-neighbor distribution described by the analytical expression [71]

$$d_1(r) = \frac{2(\lambda\pi r^2)}{r} e^{-\lambda\pi r^2}, \tag{B1}$$

where λ is the intensity of the Poisson point process. It is important to emphasize that the trend of $\langle d_1(\hat{r})\rangle_e$ ($\langle\cdots\rangle_e$ indicates the average over an ensemble) in Fig. 8(a) is not the result of a fitting procedure. Rather, it is obtained by using Eq. (B1) after calculating λ as $N/(\pi R^2)$. Here N is the number of points equal to 2000 while R is the maximum radial coordinate of the system (see the insets of Fig. 7).

Figure 8 clearly shows that two extremely different first-neighbor probability density functions characterize the two considered point processes. For a given optical density, the probability of finding two particles very close together is much larger for homogeneous random patterns (see the trend of $\langle d_1(\hat{r})\rangle_e$ near $r = 0$). On the contrary, proximity resonances do not influence Vogel spirals thanks to these peculiar geometrical properties.

APPENDIX C: REPRESENTATIVE EIGENVECTORS OF DIFFERENT LOCALIZED-RESONANCE BANDS

Figures 9(a)–9(c) display representative eigenvectors corresponding to the different classes of the scattering resonances that lead to more pronounced localization in the τ, π, and μ spirals, respectively. The spatial distributions of these quasi-modes correspond to the three eigenvalues of the Green's

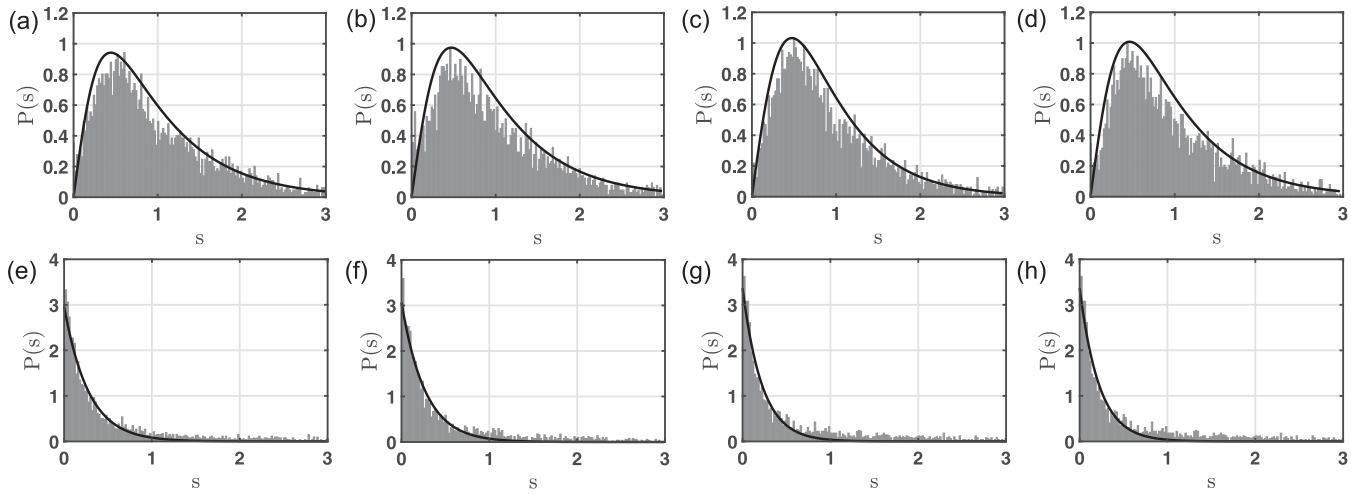

FIG. 11. Level spacing statistics of the Green's matrix eigenvalues for two different regimes: $\rho\lambda^2 = 0.1$ (panels a-d) and $\rho\lambda^2 = 10$ (panels e-h). Panels (a-e), (b-f), (c-g), (d-h) refer to the GA spiral, τ spiral, π spiral, and μ spiral configurations, respectively. The fitting curves are performed by using the critical cumulative distribution [37,38,72] (solid curves in panels (a-d)) and the Poisson distribution (solid curves in panels (e-h)).

matrix with the lower decay rates. They are labeled B_j, C_j, and D_j (with $j = 1, 2, 3$) in the τ, π, and μ configurations, respectively. In each panel of Fig. 9 the optical density is fixed to 10 and 30. Moreover, for each of them, the frequency $\hat{\omega}_n$ is also reported. We clearly observe that exactly the same spatial profile is retrieved when scanning along the dispersion branches identified by the different markers of Fig. 2. The effect of increasing the optical density $\rho\lambda^2$ is simply to produce a frequency shift in the complex scattering plane, as discussed in the main text for the GA spiral. Moreover, we notice that the spatial profiles reported in Fig. 9 agree very well with what was previously reported based on the FEM technique [53,70]. This analysis demonstrates that the different localized resonances of Fig. 2 are the different localized band edge modes produced by the strongly-fluctuating (multifractal) dispersion of the density of states in the different investigated Vogel spirals [53,70].

APPENDIX D: DIFFERENT COUPLING TERMS OF THE DYADIC GREEN PROPAGATOR

The effects of the different coupling terms of the dyadic Greens's propagator are analyzed for the τ, π, μ Vogel spirals as compared to the UR configuration. Figure 10 displays the frequency dependence of the Thouless conductance g obtained by using Eq. (5) after diagonalizing the $3N \times 3N$ Green's matrix associated to only the near-field term (panel (a)), the near-field plus the intermediate-field contribution (panel (b)), the far-field term only (panel (c)), and all the coupling contributions (panel (d)). These results are obtained for $\rho\lambda^2 = 10$. Light localization, characterized by $g < 1$, only occurs in Vogel spirals when all the coupling terms, including the near-field regime, are taken into account. This shows that light localization in Vogel spiral arrays composed of pointlike scatterers results from a collective coupling effect that involves multiple length scales.

On the other hand, homogeneous planar random media do not show any light-localization transitions when the vector nature of light is taken into account confirming the results of Refs. [8,9,16]. Indeed, the localization criterium $g(\omega) < 1$ is never satisfied in the UR configuration (see the last column of Fig. 10). Interestingly, the Thouless conductance is larger than one also when the only far-field coupling term is taken into account. Hence our findings clearly demonstrate that the absence of any structural correlations is the main responsible that prevents light localization in uniform random arrays when the vector nature of light is taken into account.

APPENDIX E: LEVEL SPACING STATISTICS IN VOGEL SPIRALS

Level statistics provides important information about electromagnetic propagation in both closed and open scattering systems. Indeed, the concept of level repulsion is related to the transport properties supported by eigenmodes because it indicates the degree of spatial overlap between them [73]. Level repulsion can help to discriminate a transition from a delocalized (presence of level repulsion) to a localized wave transport regime (absence of level repulsion). In Refs. [37,38] the distribution of level spacings was investigated in different open scattering systems for different scattering strengths. The presence of the level repulsion is characterized by the derivative of the interpolation function, called critical cumulative probability [72], while the suppression of level repulsion is indicated by the fact that the level spacings is described by the Poisson distribution [37,38,74].

The distribution of level spacings is calculated for two different optical densities (0.1 Figs. 11(a)–11(d) and 10 Figs. 11(e)–11(f)) for all the investigated Vogel spiral configurations. Figure 11 shows a clear transition between level repulsion at low optical densities and the absence of level repulsion at large optical densities. For large optical density, the distribution of level spacings follows the Poisson distribution (no level repulsion), as it occurs for uniform random systems in the localized regime [37]. On the other hand, for weakly scattering systems the level spacing distribution

follows the same critical distribution that describes the Anderson transition in random media, where wave functions feature multifractal scaling [72]. Differently from traditional uniform random media where criticality is achieved at the localization threshold, which occurs for a specific optical density in 3D, in Vogel spirals we have verified that the critical behavior occurs for a broader range of optical densities. Interestingly, this behavior was reported also for complex prime arrays [38].

APPENDIX F: AVERAGE MODAL LIFETIME

In order to address the similarities between our problem and the scattering resonances of a 2D open system we have calculated their spatial distributions and their mean lifetimes in both a 3D and a 2D environment. This analysis is summarized in Fig. 12.

Figures 12(a) and 12(b) show a comparison between representative spatial distribution of localized Green's matrix eigenvectors calculated using the cylindrical Hankel functions [17] and the dyadic formalism applied to the golden angle Vogel spiral, respectively. The 2D localized scattering resonances are very similar to the ones found in a 3D scenario. This comparison clearly shows that the geometrical nature of the 2D support determines, even in the case of 3D open systems, the spatial distribution and the localization properties of localized modes in the plane of its support. This feature allows the 2D modes to be probed by the scattering resonances of their 3D counterparts if the scattering strength is sufficiently large to induce light localization in the 2D support. However, such 3D scattering resonances have smaller average modal lifetime due to the open nature of the 3D space with respect to their 2D counterparts, as shown in Figs. 12(c) and 12(d).

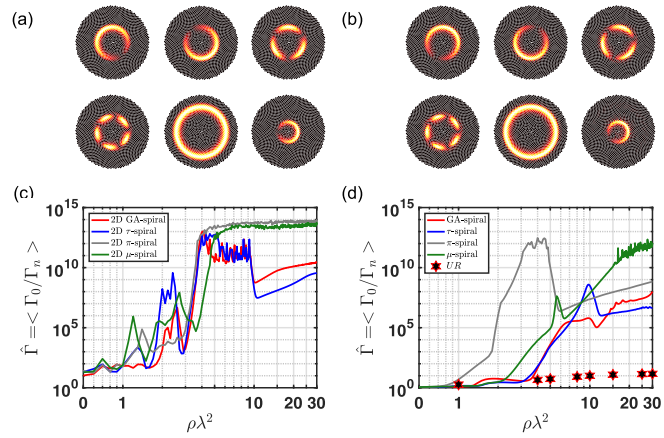

FIG. 12. Panels (a) and (b) show representative spatial distributions of localized Green's matrix eigenvectors generated by using the cylindrical Hankel functions and the dyadic formalism applied to the golden angle Vogel spiral, respectively. Panels (c) and (d) report the average modal lifetime as a function of $\rho\lambda^2$ in 2D and 3D environments, respectively.

In fact, Figs. 12(c) and 12(d) compare the average modal lifetime $\hat{\Gamma} = \langle \Gamma_0/\Gamma_n \rangle$, which determines the mean time that light spends inside a medium surrounded by vacuum [7,14], in the 2D and 3D scenarios as a function of $\rho\lambda^2$ for all the investigated spirals.

For comparison, Fig. 12(d) also reports the average modal lifetimes of uniform planar random arrays that are much smaller than the ones of Vogel spirals. This result is consistent with the fact that a light localization transition is never achieved in the random case.

[1] P. W. Anderson, Phys. Rev. **109**, 1492 (1958).
[2] A. Lagendijk, B. A. Van Tiggelen, and D. S. Wiersma, Phys. Today **62**, 24 (2009).
[3] D. S. Wiersma, Nat. Photonics **7**, 188 (2013).
[4] H. Cao, Y. G. Zhao, S. T. Ho, E. W. Seelig, Q. H. Wang, and R. P. H. Chang, Phys. Rev. Lett. **82**, 2278 (1999).
[5] D. S. Wiersma, Nat. Phys. **4**, 359 (2008).
[6] F. A. Pinheiro, Phys. Rev. A **78**, 023812 (2008).
[7] F. A. Pinheiro, M. Rusek, A. Orlowski, and B. A. Van Tiggelen, Phys. Rev. E **69**, 026605 (2004).
[8] L. Bellando, A. Gero, E. Akkermans, and R. Kaiser, Phys. Rev. A **90**, 063822 (2014).
[9] S. E. Skipetrov and I. M. Sokolov, Phys. Rev. Lett. **112**, 023905 (2014).
[10] S. E. Skipetrov, Phys. Rev. B **94**, 064202 (2016).
[11] S. E. Skipetrov and I. M. Sokolov, Phys. Rev. Lett. **114**, 053902 (2015).
[12] M. Rusek, J. Mostowski, and A. Orłowski, Phys. Rev. A **61**, 022704 (2000).
[13] M. Rusek, A. Orłowski, and J. Mostowski, Phys. Rev. E **53**, 4122 (1996).
[14] A. Lagendijk and B. A. Van Tiggelen, Phys. Rep. **270**, 143 (1996).
[15] P. Sheng, *Introduction to Wave Scattering, Localization and Mesoscopic Phenomena*, Vol. 88 (Springer Science & Business Media, Berlin, 2006).
[16] C. E. Máximo, N. Piovella, P. W. Courteille, R. Kaiser, and R. Bachelard, Phys. Rev. A **92**, 062702 (2015).
[17] M. Rusek, A. Orłowski, and J. Mostowski, Phys. Rev. E **56**, 4892 (1997).
[18] F. Riboli, F. Uccheddu, G. Monaco, N. Caselli, F. Intonti, M. Gurioli, and S. E. Skipetrov, Phys. Rev. Lett. **119**, 043902 (2017).
[19] B. A. Van Tiggelen and S. E. Skipetrov, Phys. Rev. E **73**, 045601 (2006).
[20] F. Sgrignuoli, G. Mazzamuto, N. Caselli, F. Intonti, F. S. Cataliotti, M. Gurioli, and C. Toninelli, ACS Photonics **2**, 1636 (2015).
[21] C. Vanneste and P. Sebbah, Phys. Rev. A **79**, 041802 (2009).
[22] F. Riboli, N. Caselli, S. Vignolini, F. Intonti, K. Vynck, P. Barthelemy, A. Gerardino, L. Balet, H. L. Lianhe, A. Fiore, M. Gurioli, and D. S. Wiersma, Nat. Mater. **13**, 720 (2014).
[23] N. Fayard, A. Goetschy, R. Pierrat, and R. Carminati, Phys. Rev. Lett. **120**, 073901 (2018).

[24] I. Starshynov, A. M. Paniagua-Diaz, N. Fayard, A. Goetschy, R. Pierrat, R. Carminati, and J. Bertolotti, Phys. Rev. X **8**, 021041 (2018).

[25] B. Redding, M. A. Choma, and H. Cao, Nat. Photonics **6**, 355 (2012).

[26] T. Sperling, L. Schertel, M. Ackermann, G. J. Aubry, C. M. Aegerter, and G. Maret, New J. Phys. **18**, 013039 (2016).

[27] S. E. Skipetrov and J. H. Page, New J. Phys. **18**, 021001 (2016).

[28] F. Scheffold, R. Lenke, R. Tweer, and G. Maret, Nature (London) **398**, 206 (1999).

[29] T. van der Beek, P. Barthelemy, P. M. Johnson, D. S. Wiersma, and A. Lagendijk, Phys. Rev. B **85**, 115401 (2012).

[30] R. R. Naraghi, S. Sukhov, J. J. Sáenz, and A. Dogariu, Phys. Rev. Lett. **115**, 203903 (2015).

[31] M. Kohmoto, B. Sutherland, and K. Iguchi, Phys. Rev. Lett. **58**, 2436 (1987).

[32] E. Maciá, *Aperiodic Structures in Condensed Matter: Fundamentals and Applications* (CRC Press, Boca Raton, FL, 2008).

[33] M. Razi, R. Wang, Y. He, R. M. Kirby, and L. Dal Negro, Plasmonics **14**, 253 (2019).

[34] L. Dal Negro, *Optics of Aperiodic Structures: Fundamentals and Device Applications* (Pan Stanford Publishing, Singapore, 2014).

[35] L. Dal Negro and S. V. Boriskina, Laser Photonics Rev. **6**, 178 (2012).

[36] J. Trevino, H. Cao, and L. Dal Negro, Nano Lett. **11**, 2008 (2011).

[37] L. Dal Negro, R. Wang, and F. A. Pinheiro, Crystals **6**, 161 (2016).

[38] R. Wang, F. A. Pinheiro, and L. Dal Negro, Phys. Rev. B **97**, 024202 (2018).

[39] R. Wang, M. Röntgen, C. V. Morfonios, F. A. Pinheiro, P. Schmelcher, and L. Dal Negro, Opt. Lett. **43**, 1986 (2018).

[40] L. Dal Negro and S. Inampudi, Sci. Rep. **7**, 2259 (2017).

[41] P. Barthelemy, J. Bertolotti, and D. S. Wiersma, Nature (London) **453**, 495 (2008).

[42] Z. V. Vardeny, A. Nahata, and A. Agrawal, Nat. Photonics **7**, 177 (2013).

[43] W. Gellermann, M. Kohmoto, B. Sutherland, and P. C. Taylor, Phys. Rev. Lett. **72**, 633 (1994).

[44] L. Dal Negro, C. J. Oton, Z. Gaburro, L. Pavesi, P. Johnson, A. Lagendijk, R. Righini, M. Colocci, and D. S. Wiersma, Phys. Rev. Lett. **90**, 055501 (2003).

[45] L. Mahler, A. Tredicucci, F. Beltram, C. Walther, J. Faist, H. E. Beere, D. A. Ritchie, and D. S. Wiersma, Nat. Photonics **4**, 165 (2010).

[46] H. Noh, J. K. Yang, S. V. Boriskina, M. J. Rooks, G. S. Solomon, L. Dal Negro, and H. Cao, Appl. Phys. Lett. **98**, 201109 (2011).

[47] R. Lifshitz, A. Arie, and A. Bahabad, Phys. Rev. Lett. **95**, 133901 (2005).

[48] V. M. Shalaev, *Optical Properties of Nanostructured Random Media*, Vol. 82 (Springer Science & Business Media, Berlin, 2002).

[49] F. M. Huang, Y. Chen, F. J. G. de Abajo, and N. I. Zheludev, J. Opt. A Pure Appl. Opt. **9**, S285 (2007).

[50] N. Lawrence, J. Trevino, and L. Dal Negro, J. Appl. Phys. **111**, 113101 (2012).

[51] E. F. Pecora, N. Lawrence, P. Gregg, J. Trevino, P. Artoni, A. Irrera, F. Priolo, and L. Dal Negro, Nanoscale **4**, 2863 (2012).

[52] N. Lawrence, J. Trevino, and L. Dal Negro, Opt. Lett. **37**, 5076 (2012).

[53] J. Trevino, S. F. Liew, H. Noh, H. Cao, and L. Dal Negro, Opt. Exp. **20**, 3015 (2012).

[54] S. F. Liew, H. Noh, J. Trevino, L. Dal Negro, and H. Cao, Opt. Exp. **19**, 23631 (2011).

[55] M. Naylor, Math. Mag. **75**, 163 (2002).

[56] G. J. Mitchison, Science **196**, 270 (1977).

[57] J. A. Adam, *A Mathematical Nature Walk* (Princeton University Press, Princeton, NJ, 2011).

[58] A. Capretti, G. F. Walsh, S. Minissale, J. Trevino, C. Forestiere, G. Miano, and L. Dal Negro, Opt. Express **20**, 15797 (2012).

[59] M. E. Pollard and G. J. Parker, Opt. Lett. **34**, 2805 (2009).

[60] A. Agrawal, N. Kejalakshmy, J. Chen, B. M. A. Rahman, and K. T. V. Grattan, Opt. Lett. **33**, 2716 (2008).

[61] See Supplemental Material at http://link.aps.org/supplemental/10.1103/PhysRevB.99.104202 for a description of the main structural properties of Vogel spiral arrays.

[62] L. Dal Negro, N. Lawrence, and J. Trevino, Opt. Exp. **20**, 18209 (2012).

[63] D. S. Simon, N. Lawrence, J. Trevino, L. Dal Negro, and A. V. Sergienko, Phys. Rev. A **87**, 032312 (2013).

[64] D. J. Thouless, Phys. Rep. **13**, 93 (1974).

[65] J. T. Edwards and D. J. Thouless, J. Phys. C **5**, 807 (1972).

[66] E. Abrahams, P. W. Anderson, D. C. Licciardello, and T. V. Ramakrishnan, Phys. Rev. Lett. **42**, 673 (1979).

[67] E. Abrahams, *50 Years of Anderson Localization* (World Scientific, Singapore, 2010).

[68] A. Goetschy and S. E. Skipetrov, Phys. Rev. E **84**, 011150 (2011).

[69] E. J. Heller, Phys. Rev. Lett. **77**, 4122 (1996).

[70] P. Bettotti, *Nanodevices for Photonics and Electronics: Advances and Applications* (Pan Stanford Publishing, Singapore, 2016).

[71] J. Illian, A. Penttinen, H. Stoyan, and D. Stoyan, *Statistical Analysis and Modelling of Spatial Point Patterns*, Vol. 70 (John Wiley & Sons, Chichester, West Sussex, 2008).

[72] I. K. Zharekeshev and B. Kramer, Phys. Rev. Lett. **79**, 717 (1997).

[73] M. L. Mehta, *Random Matrices*, Vol. 142 (Elsevier, San Diego, CA, 2004).

[74] F. Haake, *Quantum Signatures of Chaos*, Vol. 54 (Springer Science & Business Media, Berlin, 2013).